A comparative study on dynamic responses of spar-type floating horizontal and vertical axis wind turbines

Zhengshun Cheng [*1, 2, 4], Kai Wang[2, 3], Zhen Gao[1, 2, 4], and Torgeir Moan[1, 2, 4]

[1]Department of Marine Technology, Norwegian University of Science and Technology, Trondheim, Norway
[2]Centre for Ships and Ocean Structures, Norwegian University of Science and Technology, Trondheim, Norway
[3]NOWITECH, Norwegian University of Science and Technology, Trondheim, Norway
[4]Centre for Autonomous Marine Operations and Systems, Norwegian University of Science and Technology, Trondheim, Norway

Abstract

Interest in the exploitation of offshore wind resources using floating wind turbines has increased. Commercial development of floating horizontal axis wind turbines (FHAWTs) is emerging due to their commercial success in onshore and near-shore areas. Floating vertical axis wind turbines (FVAWTs) are also promising due to their low installation and maintenance costs. Therefore, a comparative study on the dynamic responses of FHAWTs and FVAWTs is of great interest. In the present study, a FHAWT employing the NREL 5 MW wind turbine and a FVAWT employing a Darrieus rotor, both mounted on the OC3 spar buoy, were considered. An improved control strategy was introduced for FVAWTs to achieve an approximately constant mean generator power for the above rated wind speeds. Fully coupled time domain simulations were carried out using identical, directional aligned and correlated wind and wave conditions. Due to different aerodynamic load characteristics and control strategies, the FVAWT results in larger mean tower base bending moments and mooring line tensions above the rated wind speed. Because significant two-per-revolution (2P) aerodynamic loads act on the FVAWT, the generator power, tower base bending moments and delta line tensions show prominent 2P variation. Consequently the FVAWT suffers from severe fatigue damage at the tower bottom. However, the dynamic performance of the FVAWT could be improved by increasing the number of blades , using helical blades or employing a more advanced control strategy, which requires additional research.

Key words: floating wind turbine; horizontal axis; vertical axis; dynamic response; comparative study.

*Email: zhengshun.cheng@ntnu.no

1 Introduction

In recent years, offshore wind technology has been rapidly developing with a total global installed capacity of 8.771 GW by the end of 2014 (GWE, 2015). Currently, most commercial wind farms are deployed in waters that are shallower than 50 m by using bottom-fixed supporting structures such as monopile, tripod or jacket. However, floating wind turbines are more desirable in deeper water sites, especially in the North Sea, Japan, South Korea, USA and China. Due to their commercial success onshore and near shore, floating horizontal axis wind turbines (FHAWTs) are widely used and studied with different supporting structures, including spar (Karimirad and Moan, 2012, 2011), TLP (Bachynski and Moan, 2012) and semi-submersible (Kvittem et al., 2012; Roddier et al., 2010) structures. Moreover, commercial development projects for FHAWTs are emerging, including the Kincardine and Buchan Deep projects in Scotland, the WindFloat Pacific project in the USA, and the Fukushima Forward project in Japan.

Floating vertical axis wind turbines (FVAWTs) are a very promising alternative for offshore application. Compared with FHAWTs, FVAWTs have lower centers of gravity, are independent of wind direction, and can provide reduced machine complexity. Consequently, FVAWTs may have lower operations and maintenance, support structure design, installation, and electrical infrastructure costs. Paquette and Barone (2012) indicated the potential of achieving more than 20% cost of energy (COE) reductions by using FVAWTs. Moreover, FVAWTs are more suitable for deployment on wind farms than FHAWTs. The wake generated by a pair of counter-rotating H-rotors can dissipate more quickly than the wake generated by FHAWTs, allowing them to be installed in parks with smaller separations (Kinzel et al., 2012). The average power generated by a pair of H-rotors at all azimuth angles is higher than that of an isolated turbine (Dabiri, 2011), implying that the conversion efficiency of VAWTs can be improved.

Thus, the development of FVAWTs increased and several FVAWT concepts have recently been proposed, including the DeepWind (Paulsen et al., 2015) , VertiWind (Cahay et al., 2011), Aerogenerator X (Shires, 2013; Collu et al., 2014) , and floating tilted axis (Akimoto et al., 2011) concepts. Similar to the FHAWTs, the substructures supporting the FVAWTs can be categorized as spar, semi-submersible and TLP types. A FVAWT concept with a 5 MW Darrieus rotor mounted on a semi-submersible was proposed by Wang et al. (2013), and fully coupled aero-hydro-servo-elastic simulations were carried out with emphasis on stochastic dynamic responses (Wang et al., 2016), the effects of second order difference-frequency forces and wind-wave misalignment (Wang et al., 2015a), and the emergency shutdown process with consideration of faults (Wang et al., 2014a). Dynamic response analyses were conducted for the three FVAWTs (Cheng et al., 2015a) with a 5 MW Darrieus rotor mounted on the OC3 spar buoy, the OC4 semi-submersible and a TLP designed by Bachynski and Moan (2012) by using fully coupled nonlinear time domain simulations.

Therefore it is of interest to perform comparative studies to reveal the merits and feasibilities of FHAWTs and FVAWTs. Paraschivoiu (2002) discussed the merits and disadvantages of HAWTs and VAWTs and investigated their rotor performances and support foundation loads. Eriksson et al. (2008) evaluated three different wind turbine concepts, including HAWTs and two different VAWTs with H-rotor and Darrieus rotor respectively. The comparative study emphasized the design, aerodynamic performance, type of control system, environmental impacts, noise, and manufacturing, operation and maintenance costs of these turbines. Islam et al. (2013) compared HAWTs and VAWTs regarding their footprints and highlighted the fish-schooling concept for VAWT farms. Borg et al. (2014) compared VAWTs with HAWTs by considering aspects of technology, conversion efficiency, upscaling, fatigue, machinery

position, extreme conditions and packing factors. However, the aforementioned comparisons are limited to onshore wind turbines and lack integrated dynamic response analysis.

Recently, these comparative studies were extended to floating wind turbines by several researchers. Borg and Collu (2015) further carried out a preliminary comparison between the FHAWT and FVAWT based on prime principles with emphasis on the aerodynamic forces and their impact on the static and dynamic responses. But limited comparison regarding the dynamic behavior was conducted and no controller was included for the FVAWT. Wang et al. (2014b) performed a comparative study of a FVAWT with a 5 MW Darrieus rotor and a FHAWT with the NREL 5 MW wind turbine (Jonkman et al., 2009), which were both mounted on the OC4 semi-submersible (Robertson et al., 2012). Fully coupled nonlinear simulations were carried out to investigate the dynamic responses of the FHAWT and FVAWT. Cheng et al. (2015b) studied the same rotors with OC3 spar buoys (Jonkman, 2010) subjected to constant wind. However, the wind fields were created with respect to different reference heights for the FHAWT and FVAWT,which implies that a slightly different wind field was used. Moreover, the generator power of the FVAWT exceeds 5 MW above the rated wind speed and could even reach up to 9 MW. Thus, the FHAWT and FVAWT considered in the previous comparative studies were different regarding their generator power production above the rated wind speed. Additional comparative studies of FHAWTs and FVAWTs in the same wind and wave conditions and with the same rated power, supporting platform and mooring system are needed.

In the present study, the control strategy for FVAWTs is improved to achieve an approximately constant mean generator power above the rated wind speed, which was set as 5 MW (the same as that of the FHAWT). Based on the improved controller for the FVAWT, this comparison was further extended to floating wind turbines by considering the OC3 spar floater supporting the NREL 5 MW wind turbine and a 5 MW Darrieus rotor, respectively. The ballast of the spar platform supporting the FVAWT was adjusted to retain the same draft and displacement as that of the FHAWT. A series of correlated and directionally aligned turbulent wind and wave were carried out to investigate the wind turbine performance, platform motion, structural response and mooring line tension for each floating wind turbine. This comparative study captures and demonstrates the different characteristics of these floating wind turbines and allows for detailed assessments of FHAWTs and FVAWTs.

2 Methodology

2.1 Floating Wind Turbine Models

A floating wind turbine system is usually composed of a rotor to harvest wind energy, a floating platform to support the rotor and a mooring system to hold the floater in position. The studied FHAWT and FVAWT were considered in water with a depth of 320 m, as depicted in Figure 1. The OC3 spar buoy used for the FHAWT is described in Jonkman (2010) and was used to support the NREL 5 MW wind turbine, which is a traditional three-bladed upwind HAWT (Jonkman et al., 2009). Good stability is guaranteed by the heavy ballast located at the bottom, which limits the platform pitch and roll motions under the wind and wave condition. The horizontal restoring stiffness is provided by the mooring system, as shown in Figure 1. A catenary chain mooring system with delta lines and clump weights was applied so as to increase the yaw stiffness to resist the aerodynamic yaw moment.

In this study, the same spar hull and mooring system were maintained to support a 5 MW Darrieus rotor, which was originally developed in the DeepWind project (Vita, 2011). It comprises of two blades and one rotating tower that spans from the top to the bottom which is connected to the direct drive generator. The specifications of the 5 MW Darrieus rotor and the NREL 5 MW reference wind turbine are provided in Table 1. It should be noted that the generator of the FVAWT is assumed to be located at the tower base. The mass of the rotor in the FVAWT only refers to the mass of two blades, whereas the mass of the rotor in the FHAWT comprises the masses of three blades and the hub. Due to this difference in rotor mass, the ballast of the spar hull for the FVAWT was adjusted to remain the same draft and displacement as that of the FHAWT. Because the mass difference between the two rotors is very small compared with the displacement, it is assumed that such adjustment do not significantly alter the hydrostatic performance. The geometrical, structural and hydrostatic properties of the spar floaters for the FHAWT and the FVAWT are described in Cheng et al. (2015b). In addition, free decay tests were conducted in Cheng et al. (2015b) to estimate the natural periods of rigid body motions for the floating wind turbine systems, as listed in Table 2.

Different coordinate systems are introduced to describe the dynamic responses of the two floating wind turbines. The platform motions and the tower base bending moments are all defined in the global coordinate system which originates along the tower centerline at mean sea level (MSL), as shown in Figure 1. Regarding the aerodynamic loads acting on the rotor, the thrust forces are also defined in the global coordinate system; however, the aerodynamic torque is defined with respect to the local coordinate system of the shaft with the z-axis along the shaft. This definition should be kept in mind when discussing of the differences in the aerodynamic loads.

2.2 Fully Coupled Analysis Method

Dynamic response analyses of floating wind turbine systems require sophisticated numerical tools to represent the aero-hydro-servo-elastic behaviors in time domain. Simo-Riflex-AeroDyn (Ormberg and Bachynski, 2012) and Simo-Riflex-DMS (Wang et al., 2013) are state-of-the-art fully coupled nonlinear time-domain simulation codes that can account for turbulent wind inflow, aerodynamics, hydrodynamics, control dynamics, structural dynamics and mooring line dynamics.

The FHAWT was modeled using the Simo-Riflex-AeroDyn code, which couples three computer codes to model the behavior of floating wind turbine systems in the time domain: Simo computes the rigid body hydrodynamic forces and moments on the hull; Riflex models the blades, tower, shaft and mooring lines as nonlinear finite elements, calculates the hydrodynamic loads on the mooring lines and provides links to the external controller and AeroDyn; and AeroDyn calculates the forces and moments on the blades according to the Blade Element Momentum (BEM) theory or the Generalized Dynamic Wake (GDW) theory. The external control system, which includes the generator torque controller below the rated wind speed and the blade pitch controller above the rated wind speed, was written in Java. The Simo-Riflex-AeroDyn code has been verified by comparing it with FAST and other comprehensive codes (Ormberg and Bachynski, 2012; Ormberg et al., 2011).

The FVAWT was modeled using the Simo-Riflex-DMS code, which was developed by Wang et al. (2013, 2015b). Two significant differences exist between the Simo-Riflex-DMS and Simo-Riflex-AeroDyn codes. The first difference is that the Double Multiple-Streamtube (DMS) model is employed to calculate the aerodynamic loads on the rotor in the Simo-Riflex-DMS code, rather than BEM or GDW theory,

which are used in the Simo-Riflex-AeroDyn code. The DMS model includes the effects of variations in the Reynolds number and incorporates the Beddoes-Leishman dynamic stall model. The second difference is that only a PI generator torque controller is employed to adjust the electric torque to minimize the error between the measured rotational speed and the reference rotational speed in the Simo-Riflex-DMS code. The reference rotational speed is determined according to different operational regions, which are described in detail in the next section. The DMS model has been validated by comparing it with experimental data (Wang et al., 2015b). The Simo-Riflex-DMS code has been verified by a series of numerical comparisons with computer codes HAWC2 and Simo-Riflex-AC (Cheng et al., 2016b). In the Simo-Riflex-AC, the AC code based on the actuator cylinder flow model has been validated using experimental data as well (Cheng et al., 2016a).

In both models, the spar floater was considered as a rigid body. The added mass, radiation damping and first order wave forces were obtained from a potential flow model in Wadam (Wadam, 2010). In addition, viscous forces were applied to represent the quadratic damping on the hull and mooring system, and the corresponding drag coefficients were chosen as 0.6 and 1.0 (Jonkman, 2010), respectively. The mean wave drift forces were considered and Newman's approximation was used to estimate the second-order difference-frequency wave excitation forces. The tower, blades and shaft were modeled using beam elements, and the mooring lines were represented using bar elements and connecting joints. The nonlinear finite element solver in Riflex was used for a full dynamic analysis.

2.3 Control Strategy for the FVAWT

In the previous study (Wang et al., 2014b; Cheng et al., 2015b), a baseline PI generator control, developed by Svendsen et al. (2012) and Merz and Svendsen (2013), was used to enable variable-speed and fixed-pitch operation. The architecture of the baseline controller is highlighted in the green box in Figure 2. The generator rotational speed and electric torque are measured and low-pass filtered. The controller aims to minimize the error between the measured and filtered rotational speed Ω_{mes} and the reference rotational speed Ω_{ref},

$$\Delta\Omega = \Omega_{mes} - \Omega_{ref} \tag{1}$$

in which the reference rotational speed Ω_{ref} is defined as a function of the measured and low-pass filtered electric torque $\widehat{T}$ as follows

$$\Omega_{ref} = \begin{cases} \Omega_{opt}(\widehat{T}), & \text{If } \widehat{T} < T_{\Omega_N} \left(\text{or } \widehat{V} < V_{\Omega_N}\right) \\ \Omega_N, & \text{If } \widehat{T} \geq T_{\Omega_N} \left(\text{or } \widehat{V} \geq V_{\Omega_N}\right) \end{cases} \tag{2}$$

where $\widehat{V}$ is the measured and filtered wind speed, V_{Ω_N} is the wind speed for the rated rotational speed, T_{Ω_N} is the electric torque at wind speed V_{Ω_N}, Ω_N is the rated rotational speed, and Ω_{opt} is the optimal rotational speed that can maximize the power capture. The relationship between the reference rotor rotational speed and the wind speed is illustrated in Figure 3. In the controller studied the reference rotational speed is obtained using a look-up table. The rotational speed error $\Delta\Omega$ is then fed through the proportional, integral and derivative paths to obtain an updated value of the required electric torque, as

follows,

$$T(t) = K_G\left(K_P\Delta\Omega(t) + K_I\int_0^t \Delta\Omega(\tau)d\tau + K_D\frac{d}{dt}\Delta\Omega(t)\right) \tag{3}$$

in which K_G is the generator stiffness, and K_P, K_I and K_D are the proportional, integral and derivative gains, respectively. Therefore, this controller is capable of maximizing the power capture for wind speeds below V_{Ω_N} and maintaining the rotational speed for wind speeds above V_{Ω_N}.

However, the above baseline control strategy does not limit the generator power and the generator power increases as the wind speed increases, even at above the rated wind speed V_N. At very high wind speed, very large aerodynamic thrust and torque are thus expected, which can cause large structural responses. Therefore it is of interest to figure out whether the generator power as well as aerodynamic loads on the rotor at above rated wind speed V_N should be limited.

An improved control strategy that can hold the mean generator power constant above the rated wind speed was then proposed. The reference rotational speed above the rated wind speed is determined from the measured and filtered wind speed by using a look-up table, as shown in the red box in Figure 2. In reality, it is not easy to measure the hub height wind speed directly for the FVAWT. However, as similar to the FHAWT, the tower top wind speed of the FVAWT can be easily measured. Given the wind shear that relates the wind speed at hub height and tower top, the hub height wind speed can thus be determined approximately. The look-up table was based on the relationships between the rotational speed and wind speed, which can give the constant mean aerodynamic power. A series of simulations with various fixed rotational speeds and wind speeds in the steady shear wind conditions were conducted to determine the mean aerodynamic power for the onshore rotor. Next, curve fitting based on the nonlinear least squares method was applied to obtain a curve of the rotational speed versus the wind speed for a constant mean aerodynamic power above the rated wind speed, as shown in Figure 4. The constant mean aerodynamic power was set as 5.296 MW, which was the same as that of the NREL 5MW wind turbine. Therefore, the reference rotational speed above the rated wind speed is a function of wind speed, which is the primary difference from the baseline controller. Because the look-up table is developed for an onshore rotor under steady wind conditions, the turbulent wind conditions and platform motions can both affect the aerodynamic power performance and result in small deviations in the mean aerodynamic power from the target, which will be addressed later. For turbulent wind conditions the wind speed is measured and low-pass filtered.

Similarly, the reference rotational speed for the improved controller can be written as

$$\Omega_{ref} = \begin{cases} \Omega_{opt}(\widehat{T}), & \text{If } \widehat{T} < T_{\Omega_N}\left(\text{or } \widehat{V} < V_{\Omega_N}\right) \\ \Omega_N, & \text{If } T_{\Omega_N} \le \widehat{T} < T_N\left(\text{or } V_{\Omega_N} \le \widehat{V} < V_N\right) \\ \Omega_g(\widehat{V}), & \text{if } T_N \le \widehat{T}\left(\text{or } V_N \le \widehat{V}\right) \end{cases} \tag{4}$$

where Ω_g is the rotational speed for the constant power above the rated wind speed. One example of the reference rotational speed for the onshore VAWT is the mean rotational speed as shown in Figure 6 (d).

In addition, all of the parameter values in the improved controller, except for the proportional gain K_P, were chosen to equal those used in Svendsen et al. (2012) and Merz and Svendsen (2013). Because different modeling methods are used for wind turbine systems, the proportional gain K_P was set to be 0.06 in this study to avoid low-frequency electric torque variations at very high wind speed.

2.4 Fatigue Damage Estimation

The periodic aerodynamic loads acting on the VAWT may cause considerable response oscillation for some structural components. The short-term fatigue damage of the wind turbine components is addressed in this study. A Matlab-based computer program MLife developed by NREL (Hayman, 2012) is used to estimate the short-term damage equivalent fatigue loads (DEFLs) for each component. The short-term DEFL is a constant-amplitude load that occurs at a fixed load-mean and frequency and can produce damage that is equivalent to that of the variable spectrum loads. In this study, a DEFL frequency of 1 Hz was assumed. The Wohler exponent was set to be 3 for the tower base and mooring lines. Because the studied floating wind turbines are generalized concepts, fatigue damage analysis is performed without applying the Goodman correction.

3 Load Cases

Several load cases (LCs) were defined to study the dynamic responses of the FHAWT and FVAWT, as given in Table 3-5. LC1 and LC2 were steady and turbulent wind conditions, respectively, and were used to investigate the stability and dynamic performance of the improved controller for the FVAWT. LC3 with correlated and directionally aligned wind and waves was used to compare the FHAWT and FVAWT.

For steady wind conditions, the normal wind profile (NWP) was applied, in which the wind profile $U(z)$ is the average wind speed as a function of height z above MSL, and is given by the following power law

$$U(z) = U_{ref}\left(\frac{z}{z_{ref}}\right)^{\alpha} \tag{5}$$

where U_{ref} is the reference wind speed, z_{ref} the height of reference wind speed and α the power law exponent.the value of α was chosen to be 0.14 for the floating wind turbines according to IEC 61400-3 (IEC, 2005). The values of z_{ref} were set to 90 m (hub height) and 79.78 m (vertical center of the blades) above MSL for the FHAWT and FVAWT, respectively. For turbulent wind conditions, the NWP and normal turbulence model (NTM) were both applied. The three dimensional turbulent wind fields were generated using NREL's TurbSim program (Jonkman, 2009) according to the Kaimal turbulence model for IEC Class C. The JONSWAP wave model was used to generate the wave history. The significant wave height (Hs) and peak period (Tp) were set based on their correlation with wind speed for the Statfjord site in the northern North Sea (Johannessen et al., 2002).

To obtain a more reasonable comparison of the FHAWT and FVAWT, the same wind field and wave elevation were applied to both the FVAWT and FHAWT. The reference wind speeds at hub height for the FHAWT were computed based on the FVAWT according to Equation 5, as the U_w given in Table 5. For LC2 with turbulent wind and LC3 with turbulent wind and waves, each simulation lasted 4600 s, in which the first 1000 s was removed to eliminate the start-up transient effects and to form a one-hour dynamic analysis. Five identical and independent one-hour simulations with different seeds for turbulent winds and irregular waves were carried out for each LC to reduce the stochastic variations. The comparative study was based on the statistical values obtained from the simulations. The mean value and standard

deviation of the dynamic responses were obtained by averaging the mean values and standard deviations of the five one-hour ensembles.

4 Results and Discussion

4.1 Performance of the Improved Controller for the FVAWT

Prior to the comparative study of the FHAWT and FVAWT, a series of steady and turbulent wind conditions were conducted to study the stability and dynamic performances of the improved controller. Figure 5 demonstrates the mean value of the generator power and thrust for the onshore HAWT and VAWT with baseline and improved control strategies in the steady wind condition. Compared with the baseline controller, the improved controller for the VAWT greatly reduces the generator power above the rated wind speed and can maintain an approximately constant mean generator power at 5 MW, which can be regarded as the rated power. Due to the variations of the aerodynamic torque, the generator power could be larger than 5 MW. Furthermore, the improved controller for the VAWT could decrease the aerodynamic thrust acting on the rotor, and help reduce the structural responses such as the tower base fore-aft bending moments. However, the mean thrust of the VAWT is much larger than that of the HAWT above the rated wind speed, implying that the VAWT may have a much larger structural response despite the relatively shorter torque arm.

In addition, the effect of wind turbulence on the wind turbine performance for the onshore and floating VAWT with the improved controller were investigated, as shown in Figure 6. Figure 6 presents the mean values and standard deviations of the generator power, thrust, aerodynamic torque and rotational speed for onshore and floating VAWTs with the improved controller under steady and turbulent wind conditions. The responses are plotted against the mean wind speed.

The steady state generator power and rotational speed of the onshore VAWT above the rated wind speed follow the curve implemented in the controller, but there is a small reduction in the generator power of the spar FVAWT above the rated wind speed under steady wind conditions, which is due to the tower tilt caused by the platform roll and pitch motions and the reduced standard deviation of rotational speed. Under turbulent wind conditions, the mean values of the rotational speed can follow the pre-calculated curve above the rated wind speed; however, the standard deviations increase significantly in turbulent wind conditions, and are approximately 50% larger than those during steady wind conditions. Consequently, the mean values of the generator power and aerodynamic torque increase slightly under turbulent wind conditions, and their standard deviations significantly increase. Despite these large fluctuations, the mean values of the generator power for the spar FVAWT reach 5 MW under turbulent wind conditions and vary slightly around 5 MW as the mean wind speed increases. Therefore, the improved controller used in this study shows good stability with respect to the mean generator power performance, and can be applied to conduct comparative studies on the dynamic responses of the FHAWT and FVAWT in turbulent wind and wave conditions.

4.2 Performance in Turbulent Wind and Wave Conditions

4.2.1 Wind Turbine Performance

Figure 7 shows the mean values and standard deviations of generator power, aerodynamic thrust and torque, and rotational speed for the FHAWT and FVAWT. The rated wind speed for the FHAWT and FVAWT are 11.4 m/s and 14 m/s, respectively. Above the rated wind speed, the mean generator powers of the FHAWT and FVAWT are very close to the rated power of 5 MW, which makes the comparison between the FHAWT and FVAWT more reasonable. For wind speeds below 14 m/s, the mean generator power of the FHAWT is always much greater than that of the FVAWT due to the higher power coefficient. Because the long-term wind speeds commonly follow the Weibull distribution with the majority below 14 m/s (Johannessen et al., 2002), the FHAWT can harvest more wind energy than the FVAWT during the same period; However, a yaw control device is also required for the FHAWT as the winds are generally not unidirectional, while VAWT is independent of wind direction.

Different control strategies were applied to the FHAWT and FVAWT, respectively. For the FHAWT, the generator-torque controller and the blade-pitch controller with constant torque were employed below and above the rated wind speed of 11.4 m/s, respectively, which caused the maximum thrust to occur at the rated wind speed and a constant torque above the rated wind speed, as shown in Figure 7 (b) and (c). Regarding the FVAWT, only the generator-torque controller was used as described above and both the mean aerodynamic thrust and torque increased as the wind speed increased.

Figure 7 (d) presents the mean value and standard deviation of the rotor rotational speeds of the FHAWT and FVAWT. The mean rotational speed for the FVAWT above the rated wind speed follows a predetermined curve to achieve an approximately constant generator power, as illustrated in Figure 7 (a). It is very interesting to observe that the FHAWT has not only a much larger standard deviation of the rotational speed, but also a much smaller standard deviation of the generator power. This is due to more stable aerodynamic loads acting on the rotor (standard deviations are given in Figure 7 (b) and (c)). The characteristics of the aerodynamic loads acting on the rotor of the spar-type FHAWT and FVAWT have also been studied in Cheng et al. (2015b) and Wang et al. (2014b). Because the azimuthal angle of the shaft varies periodically in the FVAWT at the rotational speed, the angle of attack encountered by each blade changes correspondingly, leading to the periodic fluctuations in the aerodynamic load on each blade. The rotational frequency corresponding to the rotational speed can be denoted as the 1P frequency. Thus, the resulting aerodynamic loads for the considered 2-bladed FVAWT are considered to vary with the 2P frequency. Moreover, the thrust and aerodynamic torque range from approximate zero to double the mean value.

4.2.2 Platform Motions

Due to the difference in the aerodynamic load acting on the rotor and the dynamic characteristics of the two concepts, the FVAWT and FHAWT have different platform motions. Figure 8 shows the mean value and standard deviation of the surge, roll, pitch and yaw motions of the FVAWT and FHAWT. The trends in the mean values of the surge, heave and pitch are very similar to those of the mean thrust acting on the rotors of the FHAWT and FVAWT. This is because that the mean values of the platform motions are mainly related to wind thrust force. As the center of gravity of the spar buoy is more than 70 m below MSL and the fairleads are located well below the line of action of the aerodynamic forces, the pitch

motion contributes a lot to the surge motion, resulting in much larger surge motions for the FHAWT and FVAWT. The mean values of the sway, roll and yaw motions of the FHAWT are very small, because the aerodynamic lateral force and yaw moment are small due to symmetry. However, the FVAWT has much larger mean values in sway, roll and yaw motions, especially at high wind speed. The sway and roll motions are caused by the aerodynamic lateral force that acts on the rotor, and the much larger yaw motion results from the aerodynamic torque acting on the rotor of the FVAWT, which leads to the considerable yaw moment on the spar hull.

Despite the significant fluctuations of the aerodynamic loads acting on the FVAWT, the standard deviation of the platform motions for the FVAWT are the same order of magnitude as those of the FHAWT. Although the standard deviation of thrust for the FHAWT is much smaller than that of the FVAWT, the standard deviations of surge and pitch motions for the FHAWT are larger than those of the FVAWT below the rated wind speed of 11.4 m/s, due to the larger surge and pitch responses that results from the low-frequency turbulent wind, the difference-frequency wave force and the first order wave force, as shown in Figure 9 for LC3.3. The FHAWT has a larger wave-induced pitch resonant response and wave frequency response than the FVAWT. Moreover, the response corresponding to the 2P frequency of the surge and pitch motions can be clearly observed for the FVAWT, but their contributions to the standard deviation are very small. However, above the rated wind speed, the surge and pitch responses due to the low-frequency turbulent wind become increasing dominating for the FVAWT, as shown in Figure 10. Consequently, the standard deviations of the surge and pitch motions of the FVAWT are much larger than those of the FHAWT. In addition, the yaw response of the FHAWT is mainly induced by the low-frequency turbulent wind, while that of the FVAWT is primarily excited by the low-frequency turbulent wind and the 2P aerodynamic torque.

4.2.3 Tower Base Bending Moments

It was assumed that the tower bottom considered for the FVAWT was located below the bearings of the generator shaft. The detailed structural design of the connection is not considered here. For the FHAWT and the FVAWT, the tower base bending moments are both driven by the aerodynamic loads acting on the rotor and by the weight of the rotor, which can result in a large bending moment due to platform pitch or tower bending. Here both the tower base fore-aft bending moment and the side-to-side bending moment were studied.

Figure 11 shows the power spectra of the tower base fore-aft and side-to-side bending moment for the FHAWT and FVAWT in LC3.5. Obviously the response corresponding to the 2P frequency is considerably dominating in the tower base fore-aft and side-to-side bending moments for the FVAWT. As illustrated above, the aerodynamic loads acting on the FVAWT vary significantly and periodically with the azimuthal angle of the rotor, which can result in considerable variations in the tower base bending moment. Moreover, the tower base fore-aft bending moment for the FVAWT also includes prominent low-frequency turbulent wind induced response and wave frequency response. With respect to the FHAWT, the tower base fore-aft bending moment consists of significant low-frequency turbulent wind induced response, pitch resonant response and wave frequency response. The pitch resonant response mainly results from the relatively large platform pitch motion. In addition, the tower base of the FHAWT is mainly affected by the fore-aft bending moment, while the side-to-side bending moment can be neglected.

Both the extreme structural response and fatigue damage, which are related to the maximum value

and standard deviation of the structural responses, respectively, are of concern for floating wind turbines. Figure 12 compares the mean values, standard deviations and maximum values of the tower base fore-aft and side-to-side bending moments for the FHAWT and FVAWT under different loads. The mean values, standard deviations and maximum values of the tower base bending moments for the FVAWT, except for the mean values below the rated wind speed, are much larger than those of the FHAWT. Thus the tower base of the FVAWT will suffer relatively larger fatigue damage than that of the FHAWT, as shown by the 1 Hz DEFLs in Figure 13. The DEFL of the fore-aft bending moment for the FVAWT above the rated wind speed is approximately twice that of the FHAWT. Moreover, the DEFL of the side-to-side bending moment for the FVAWT is more than six times greater than that of the FHAWT.

4.2.4 Mooring Line Tensions

In this study, identical catenary chain mooring systems with delta lines and clump weights were applied to the FHAWT and FVAWT. Each mooring line is composed of two upper delta lines, a upper line, a clump mass and a lower line, as shown in Figure 1. The lower line tension and delta line tension at the three anchor points and the three fairlead points are studied here. Only the normal operational conditions are considered in the present study. Extreme conditions and fault conditions will be studied in the future.

The lower line tensions are compared for the FHAWT and FVAWT in Figure 14, including the mean value, standard deviation and maximum value. The mean value of the lower line tensions is primarily wind-induced. Because wind moves in the positive x direction, the tensions in the lower lines 2 and 3 are much larger than that in lower line 1. Moreover, due to the larger mean thrust below the rated wind speed, the tensions in lower lines 2 and 3 for the FHAWT are slightly larger than those for the FVAWT. Similarly, above the rated wind speed the lower line tensions in mooring lines 2 and 3 of the FVAWT are larger than those of the FHAWT as a result of the much larger mean thrust, as shown in Figure 7(b). However, the discrepancy in the lower line tensions between the FHAWT and the FVAWT is very small compared to the mean value.

The tensions in the delta lines for the FHAWT and FVAWT are also of concern, especially for the FVAWT at high wind speeds as shown in Figure 16. Due to the large yaw motion experienced by the FVAWT above the rated wind speed, the mean values of tension among the six delta lines vary significantly. In LCs 3.7 and 3.8, the mean tension in delta line 3a reaches approximately 1588 kN, which is very similar to the largest mean tension in the lower line 3.

Figure 15 shows the power spectra of the tension in lower line 2 and delta line 2a for the FHAWT and the FVAWT at LC3.3 and LC3.7, respectively. The low-frequency turbulent wind induced response of mooring line tension is always very dominating for the FHAWT and FVAWT. In LCs with higher significant wave height, the wave frequency responses in the delta line tensions and in the lower line tensions have become more obvious for both the FHAWT and FVAWT. Significant pitch resonant responses are also excited in the delta lines for the FHAWT and FVAWT.

In addition, the 2P response is observed in the delta lines for the FVAWT and increases significantly as the wind speed increases. However, despite the prominent 2P response in the delta line tensions, the corresponding 2P response in the lower line tensions is negligible, because the catenary mooring lines can absorb the 2P excitations and alleviate or even dampen out the 2P response in the lower line tensions.

Fatigue damages of the lower lines and delta lines are also studied using the MLife code, as the 1 Hz tension DEFLs show in Figure 17. The DEFLs of the tension in the lower lines are obviously close to

each other for the FVAWT and FHAWT. However, in the delta lines, the DEFLs of the tension for the FVAWT are much larger than the FHAWT in delta lines 2a, 2b, 3a and 3b above the rated wind speed.

5 Conclusions

This paper deals with a comparative study on the dynamic responses of a FHAWT and FVAWT, with identical spar buoys and catenary mooring systems. The FHAWT uses the NREL 5 MW reference wind turbine, while the FVAWT employs a 5 MW Darrieus rotor. It should be noted that it is a preliminary comparison, since the DeepWind rotor used in this work is not as optimized as the HAWT and the FVAWT can be further improved. Due to the difference in rotor mass, the ballast of the spar for the FVAWT was adjusted to maintain the same draft and displacement as that of the FHAWT. Fully coupled time domain simulations were carried out to study the dynamic responses using the state-of-the-art codes Simo-Riflex-AeroDyn and Simo-Riflex-DMS for the FHAWT and FVAWT, respectively. The same environmental conditions with directionally aligned and correlated wind and wave were applied for the FHAWT and FVAWT.

An improved control strategy for the FVAWT is introduced first to maintain an approximately constant generator power above the rated wind speed. This control was achieved by determining the reference rotational speed as a function of the measured hub height wind speed based on a pre-calculated curve of the rotational speed versus the wind speed. The improved controller can help hold the mean generator power approximately constant for onshore and floating VAWTs above the rated wind speed, regardless of the presence of steady or turbulent wind conditions. However, during turbulent wind conditions, the standard deviations of the generator power and rotational speed are much larger. Due to the improved controller, the rated power for the FHAWT and FVAWT are very close to each other, which makes the comparative study more reasonable. Using the improved controller for the FVAWT, a series of simulations were conducted to investigate the response characteristics for the FHAWT and FVAWT, including the wind turbine performance, platform motions, tower base bending moments and mooring line tensions.

Due to the higher power coefficient, the FHAWT can harvest more wind energy below the rated wind speed than the FVAWT. However, the aerodynamic loads acting on the 2-bladed FVAWT show significant periodic variations compared with those of the FHAWT. Consequently, the variations of the generator power for the FVAWT are much larger. The variations of the aerodynamic loads are expected to be mitigated by increasing the blade number or introducing helical blades at the cost of higher manufacturing costs. More advanced control strategies, such as model predictive control, are also possible for the FVAWT. All of these strategies can help alleviate the variations in generator power for the FVAWT.

For the above rated wind speed, the increasing aerodynamic loads for the FVAWT result in much larger platform motions, especially in surge, pitch and yaw. However, despite the considerable fluctuations of the aerodynamic loads, the standard deviations of the platform motions for the FVAWT are only slightly larger than those of the FHAWT. The motion responses are dominated by the low-frequency wind induced response, motion resonant response and wave frequency response.

Regarding the structural response, such as the tower base bending moment, the 2P responses of the fore-aft and side-to-side bending moments of the FVAWT are dominant. However, for the FHAWT the pitch resonant response of the fore-aft bending moment is dominant. All of the mean values, standard

deviations and maximum values of the tower base bending moments for the FVAWT, except the mean values below the rated wind speed, are much larger than those for the FHAWT. Moreover, the FVAWT can suffer larger fatigue damage than the FHAWT.

The mean values of the mooring line tensions are mainly wind-induced. In the lower line, the mean value, standard deviation and maximum value of the tension of the FVAWT are close to those of the FHAWT at low and mediate wind speeds. However, at very high wind speeds the tensions in mooring line 2 and 3 for the FVAWT are larger than those for the FHAWT. In the delta line, the tensions for the FVAWT vary significantly among delta lines due to the large yaw motion experienced. Moreover, prominent 2P response and wave frequency response are observed in the delta line tension in the LCs with higher significant wave height and higher wind speed. The corresponding 2P and wave frequency responses in the lower line tension are very small due to the mitigation of the catenary mooring lines and clump weights.

Although the spar buoy and the mooring system are originally designed to support the NREL 5 MW wind turbine, it is still reasonable to use them to support the Darrieus rotor because the hydrostatic performance does not change very much with small differences in the rotor mass when compared with the displacement. By minimizing the differences between the FHAWT and FVAWT, this comparative study illustrates the dynamic response characteristics of each concept and can serve as a basis for their further development.

Acknowledgments

The authors would like to acknowledge the financial support from the EU FP7 project MARE WINT (project NO. 309395) through the Centre for Ships and Ocean Structures (CeSOS) and Centre for Autonomous Marine Operations and Systems (AMOS) at the Department of Marine Technology, Norwegian University of Science and Technology (NTNU), Trondheim, Norway. The first author would also like to thank Dr. Erin Bachynski from MARINTEK for kindly helping with using the simulation codes.

References

Global wind statistics 2014, Global Wind Energy Council, 2015.

H. Akimoto, K. Tanaka, and K. Uzawa. Floating axis wind turbines for offshore power generationâĂŤa conceptual study. *Environmental Research Letters*, 6(4):044017, 2011. doi: 10.1088/1748-9326/6/4/044017.

E. Bachynski and T. Moan. Design considerations for tension leg platform wind turbines. *Marine Structures*, 29(1):89–114, 2012. doi: 10.1016/j.marstruc.2012.09.001.

M. Borg and M. Collu. A comparison between the dynamics of horizontal and vertical axis offshore floating wind turbines. *Philosophical Transactions of the Royal Society of London A: Mathematical, Physical and Engineering Sciences*, 373(2035):20140076, 2015. doi: 10.1098/rsta.2014.0076.

M. Borg, A. Shires, and M. Collu. Offshore floating vertical axis wind turbines, dynamics modelling state of the art. part i: Aerodynamics. *Renewable and Sustainable Energy Reviews*, 2014. doi: 10.1016/j.rser.2014.07.096.

M. Cahay, E. Luquiau, C. Smadja, and F. Silvert. Use of a vertical wind turbine in an offshore floating wind farm. In *Offshore Technology Conference*, Houston, Texas, USA, 2011.

Z. Cheng, K. Wang, Z. Gao, and T. Moan. Dynamic response analysis of three floating wind turbine concepts with a two-bladed darrieus rotor. *Journal of Ocean and Wind Energy*, 2:213–222, 2015a. doi: 10.17736/jowe.2015.jcr33.

Z. Cheng, K. Wang, Z. Gao, and T. Moan. Comparative study of spar type floating horizontal and vertical axis wind turbines subjected to constant winds. In *Proceedings of EWEA Offshore 2015*, Copenhagen, Denmark, 2015b.

Z. Cheng, H. A. Madsen, Z. Gao, and T. Moan. Aerodynamic modeling of floating vertical axis wind turbines using the actuator cylinder method. *Submitted to Energy Procedia*, 2016a.

Z. Cheng, H. A. Madsen, Z. Gao, and T. Moan. A fully coupled method for numerical modeling and dynamic analysis of floating vertical axis wind turbines. *Submitted to Renewable Energy*, 2016b.

M. Collu, F. P. Brennan, and M. H. Patel. Conceptual design of a floating support structure for an offshore vertical axis wind turbine: the lessons learnt. *Ships and Offshore Structures*, 9(1):3–21, 2014. doi: 10.1080/17445302.2012.698896.

J. O. Dabiri. Potential order-of-magnitude enhancement of wind farm power density via counter-rotating vertical-axis wind turbine arrays. *Journal of Renewable and Sustainable Energy*, 3(4):043104, 2011. doi: 10.1063/1.3608170.

S. Eriksson, H. Bernhoff, and M. Leijon. Evaluation of different turbine concepts for wind power. *Renewable and Sustainable Energy Reviews*, 12(5):1419–1434, 2008. doi: http://dx.doi.org/10.1016/j.rser.2006.05.017.

G. Hayman. Mlife theory manual for version 1.00, 2012.

IEC. International standard 61400-1, wind turbines, part 1: Design requirements, 2005.

M. Islam, S.Mekhilef, and R.Saidur. Progress and recent trends of wind energy technology. *Renewable and Sustainable Energy Reviews*, 21:456–468, 2013. doi: 10.1016/j.rser.2013.01.007.

K. Johannessen, T. S. Meling, and S. Haver. Joint distribution for wind and waves in the northern north sea. *International Journal of Offshore and Polar Engineering*, 12(1), 2002.

B. J. Jonkman. Turbsim user's guide: Version 1.50., 2009.

J. Jonkman. Definition of the floating system for phase IV of OC3. Tech. Rep. NREL/TP-500-47535, NREL, Golden, CO, USA, 2010.

J. M. Jonkman, S. Butterfield, W. Musial, and G. Scott. Definition of a 5-mw reference wind turbine for offshore system development. Tech. Rep. NREL/TP-500-38060, NREL, Golden, CO, USA, 2009.

M. Karimirad and T. Moan. Extreme dynamic structural response analysis of catenary moored spar wind turbine in harsh environmental conditions. *Journal of Offshore Mechanics and Arctic Engineering*, 133(4):041103, 2011. ISSN 08927219. doi: 10.1115/1.4003393.

M. Karimirad and T. Moan. Wave and wind induced dynamic response of a spar-type offshore wind turbine. *Journal of Waterway, Port, Coastal, and Ocean Engineering*, 138(1):9âĂŞ20, 2012. doi: 10.1061/(asce)ww.1943-5460.

M. Kinzel, Q. Mulligan, and J. O. Dabiri. Energy exchange in an array of vertical-axis wind turbines. *Journal of Turbulence*, 13(38):1–13, 2012. doi: 10.1080/14685248.2013.825725.

M. I. Kvittem, E. E. Bachynski, and T. Moan. Effects of hydrodynamic modelling in fully coupled simulations of a semi-submersible wind turbine. *Energy Procedia*, 24:351–362, 2012. doi: 10.1016/j.egypro.2012.06.118.

K. O. Merz and H. G. Svendsen. A control algorithm for the deepwind floating vertical-axis wind turbine. *Journal of Renewable and Sustainable Energy*, 5(6):063136, 2013. doi: 10.1063/1.4854675.

H. Ormberg and E. E. Bachynski. Global analysis of floating wind turbines: Code development, model sensitivity and benchmark study. In *Proceedings of the 22th International Offshore and Polar Engineering Conference*, Rhodes, Greece, 2012.

H. Ormberg, E. Passano, and N. Luxcey. Global analysis of a floating wind turbine using an aero-hydro-elastic model: Part 1 code development and case study. In *Proceedings of the 30th International Conference on Ocean, Offshore and Arctic Engineering*, Rotterdam, The Netherlands, 2011.

J. Paquette and M. Barone. Innovative offshore vertical-axis wind turbine rotor project. In *EWEA 2012 Annual Event*, Copenhagen, Denmark, 2012.

I. Paraschivoiu. *Wind turbine design: with emphasis on Darrieus concept*. Polytechnic International Press., Montreal, Canada., 2002.

U. S. Paulsen, M. Borg, H. A. Madsen, T. F. Pedersen, J. Hattel, E. Ritchie, C. S. Ferreira, H. Svendsen, P. A. Berthelsen, and C. Smadja. Outcomes of the deepwind conceptual design. *Energy Procedia*, 80: 329–341, 2015. doi: 10.1016/j.egypro.2015.11.437.

A. Robertson, J. Jonkman, M. Masciola, H. Song, A. Goupee, A. Coulling, and C. Luan. Definition of the semisubmersible floating system for phase II of OC4, 2012.

D. Roddier, C. Cermelli, A. Aubault, and A. Weinstein. Windfloat: A floating foundation for offshore wind turbines. *Journal of Renewable and Sustainable Energy*, 2(3):033104, 2010. doi: 10.1063/1.3435339.

A. Shires. Design optimisation of an offshore vertical axis wind turbine. *Proceedings of the ICE-Energy*, 166(EN1):7–18, 2013.

H. G. Svendsen, K. O. Merz, and A. G. Endegnanew. Control of floating vertical axis wind turbine. In *European Wind Energy Conference and Exhibition*, Copenhagen, Denmark, 2012.

L. Vita. *Offshore Floating Vertical Axis Wind Turbines with Rotating Platform*. Phd thesis, Technical University of Denmark, 2011.

Wadam. Wave analysis by diffraction and morison theory. *SESAM user manual. Det Norske Veritas, Høvik*, 2010.

K. Wang, T. Moan, and M. O. L. Hansen. A method for modeling of floating vertical axis wind turbine. In *Proceedings of the 32th International Conference on Ocean, Offshore and Arctic Engineering*, Nantes, France, 2013.

K. Wang, M. O. L. Hansen, and T. Moan. Dynamic analysis of a floating vertical axis wind turbine under emergency shutdown using hydrodynamic brake. *Energy Procedia*, 53:56–69, 2014a.

K. Wang, C. Luan, T. Moan, and M. O. L. Hansen. Comparative study of a FVAWT and a FHAWT with a semi-submersible floater. In *Proceedings of the 24th International Ocean and Polar Engineering Conference*, Busan, South Korea, 2014b.

K. Wang, Z. Cheng, T. Moan, and M. O. L. Hansen. Effect of difference-frequency forces on the dynamics of a semi-submersible type FVAWT in misaligned wave-wind condition. In *Proceedings of the 25th International Ocean and Polar Engineering Conference*, Kona, Big Island, Hawaii, USA, 2015a.

K. Wang, M. Hansen, and T. Moan. Model improvements for evaluating the effect of tower tilting on the aerodynamics of a vertical axis wind turbine. *Wind Energy*, 18:91–110, 2015b. doi: 10.1002/we.1685.

K. Wang, T. Moan, and M. O. L. Hansen. Stochastic dynamic response analysis of a floating vertical-axis wind turbine with a semi-submersible floater. *Wind Energy*, 2016. doi: 10.1002/we.1955.

List of Figures

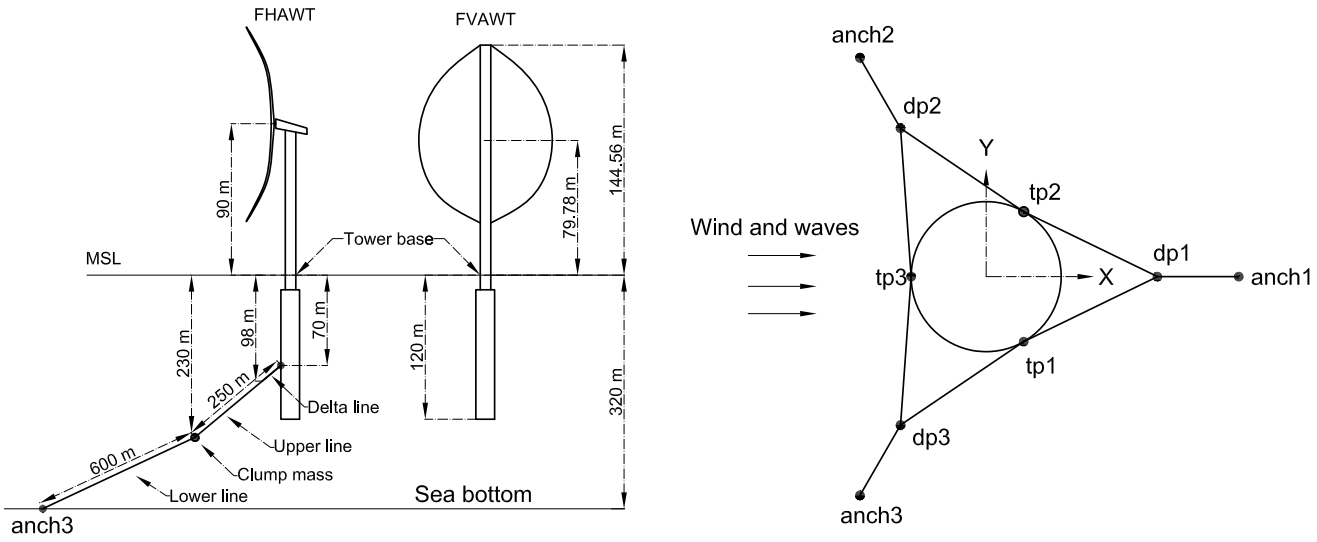

Figure 1: Schematic of the floating wind turbines and mooring system

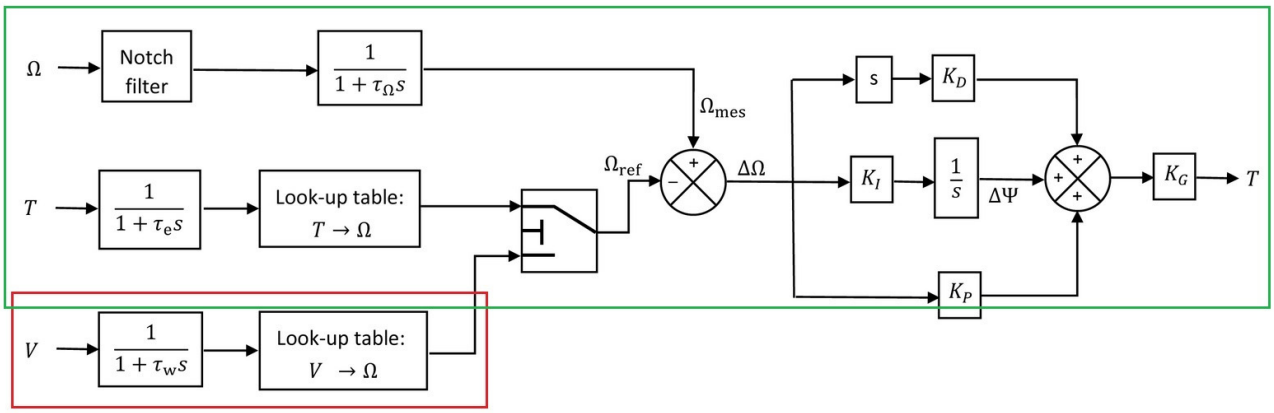

Figure 2: The generator torque control algorithm for FVAWT based on a PID architecture.

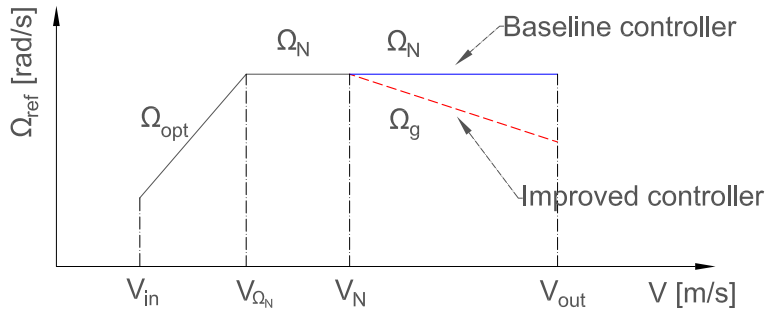

Figure 3: The relationship between the reference rotor rotational speed and the wind speed for the baseline and improved controllers

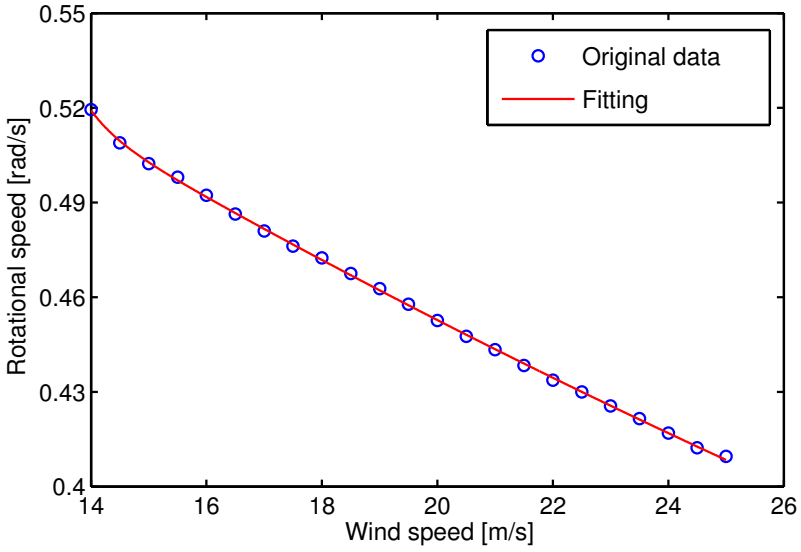

Figure 4: The relationship between the rotational speed and the wind speed for the considered Darrieus rotor with a constant mean aerodynamic power of 5.296 MW for the above rated wind speed

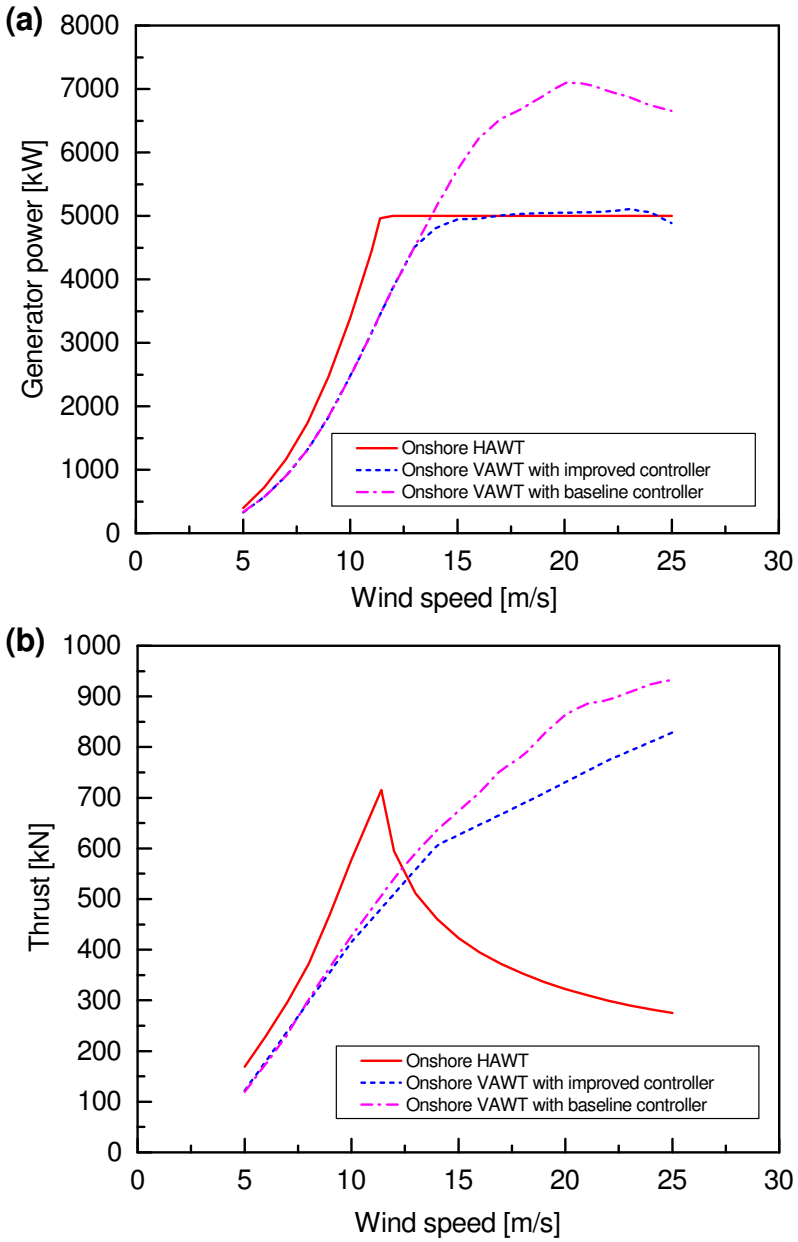

Figure 5: Steady-state mean generator power and thrust of the onshore HAWT and VAWT with different control strategies

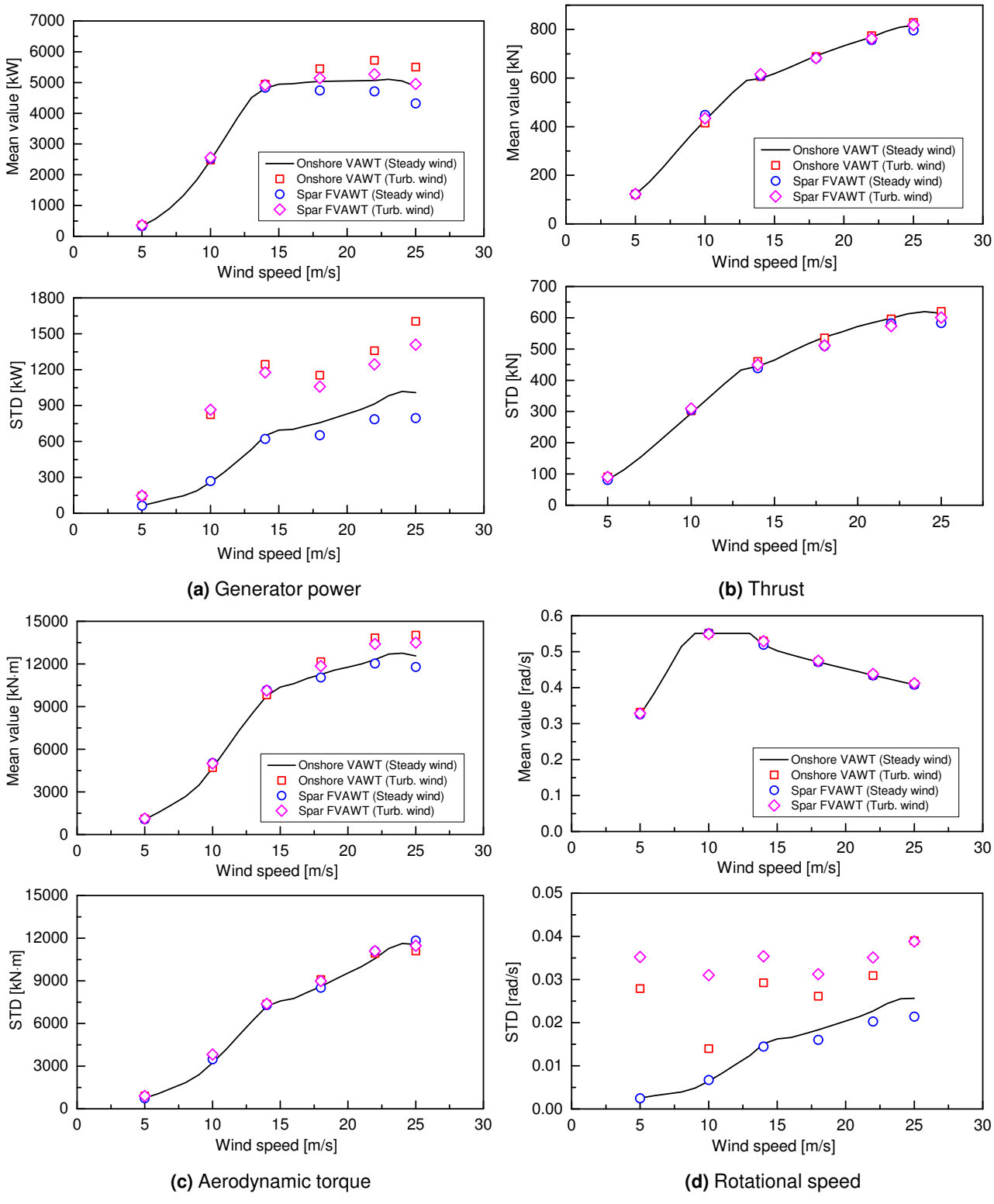

Figure 6: Mean values and standard deviations of the generator power, thrust, aerodynamic torque and rotational speed for landbased VAWT and spar-type FVAWT with the improved control strategy for steady and turbulent wind conditions.

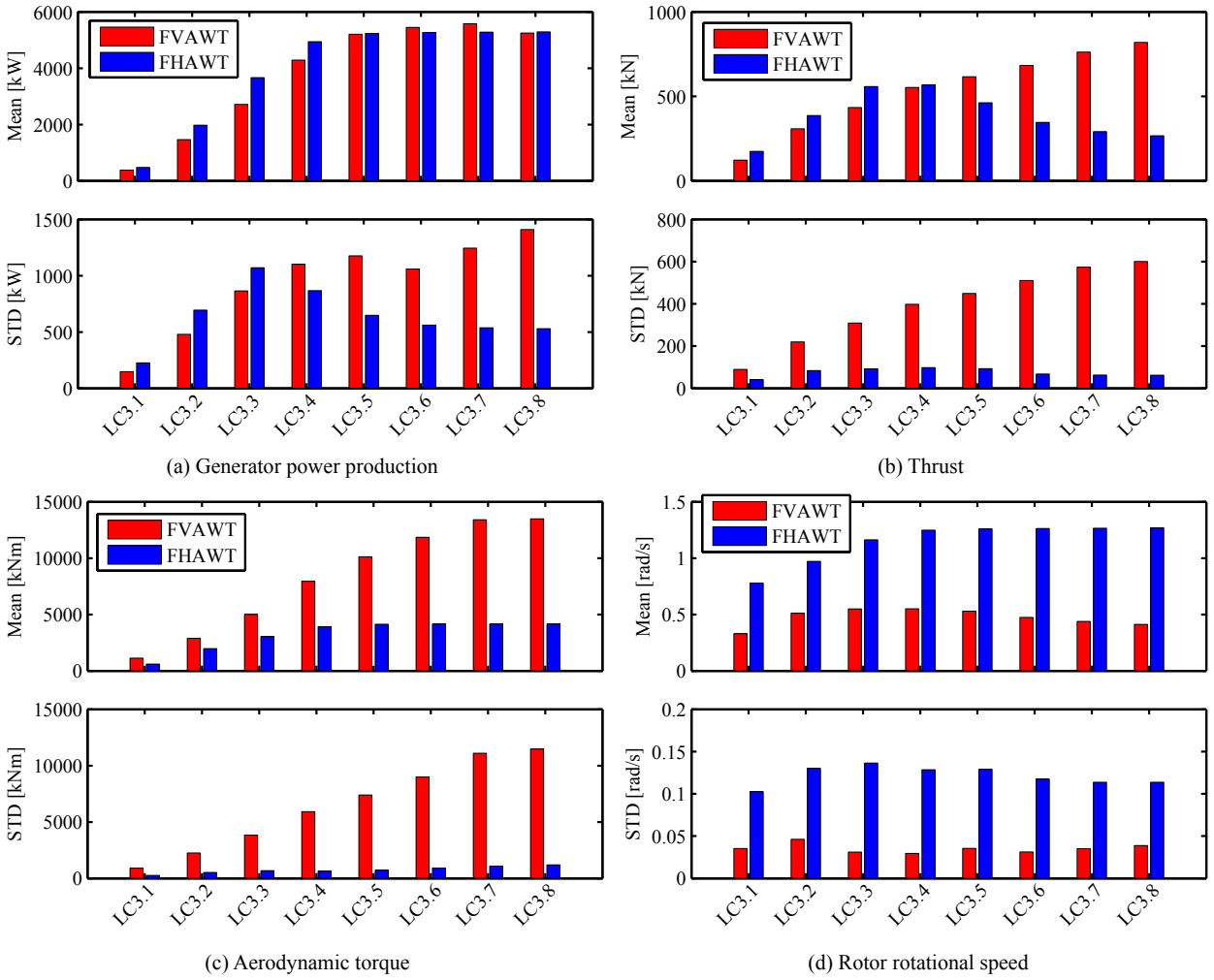

Figure 7: Mean values and standard deviations of (a) generator power, (b) thrust, (c) aerodynamic torque and (d) rotational speed for the FHAWT and FVAWT under turbulent wind conditions.

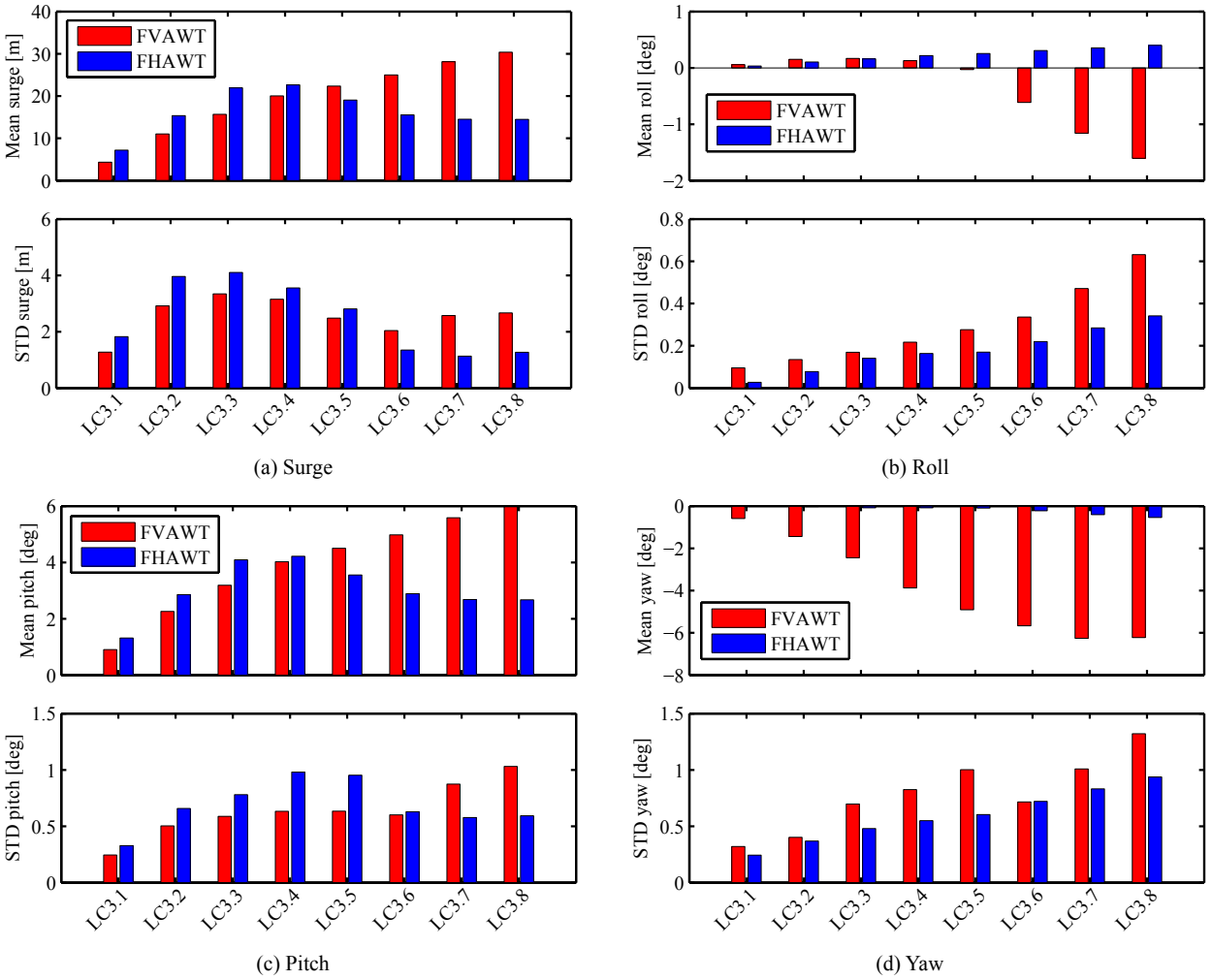

Figure 8: Mean values and standard deviations of the platform (a) surge, (b) roll, (c) pitch, (d) yaw motions for the FHAWT and FVAWT under turbulent wind conditions.

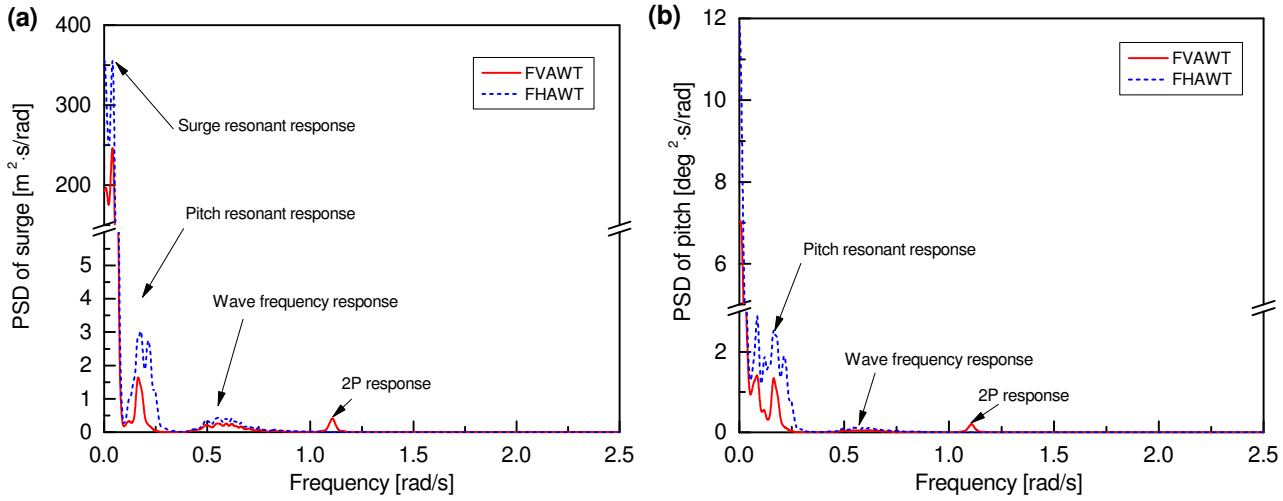

Figure 9: Power spectra of the platform (a) surge and (b) pitch motions for the FHAWT and FVAWT in LC3.3 with U_w=10 m/s.

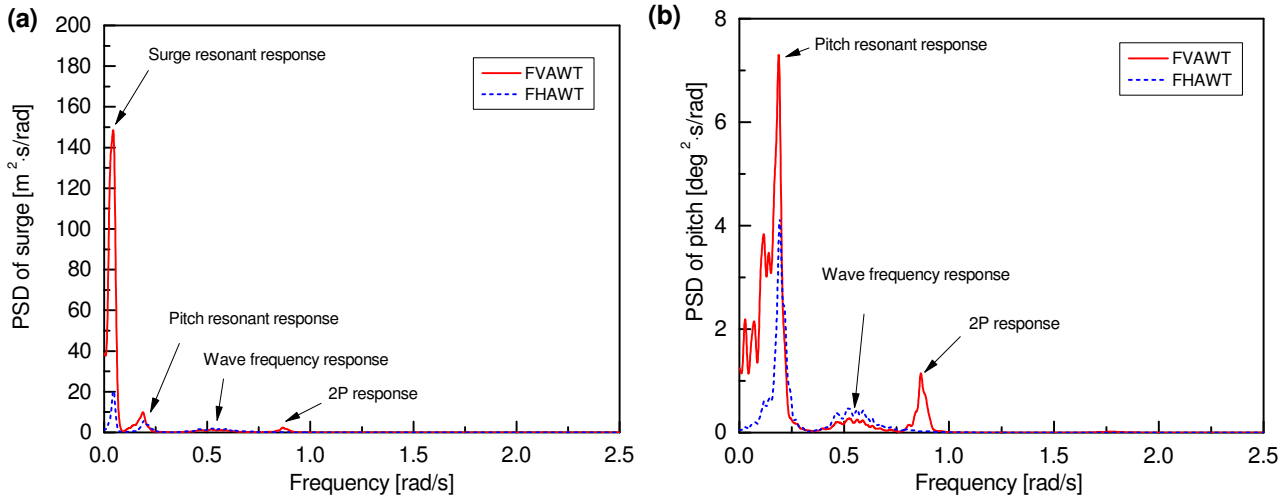

Figure 10: Power spectra of the platform (a) surge and (b) pitch motions for the FHAWT and FVAWT in LC3.7 with U_w=22 m/s.

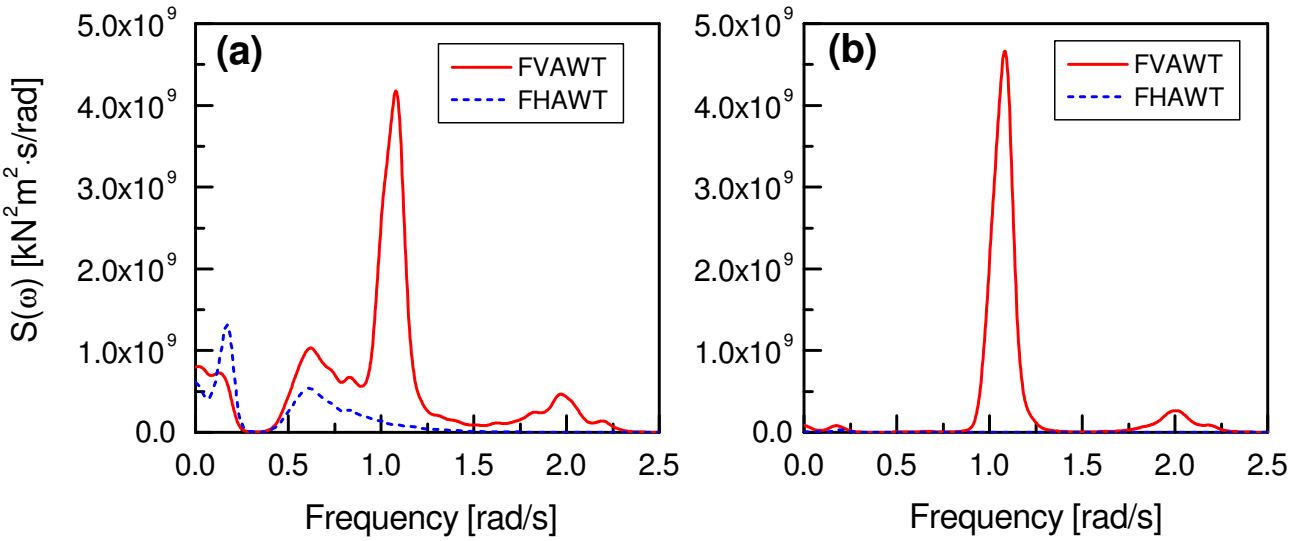

Figure 11: Power spectra of the tower base (a) fore-aft bending moment and (b) side-to-side bending moment for the FHAWT and FVAWT in LC3.5

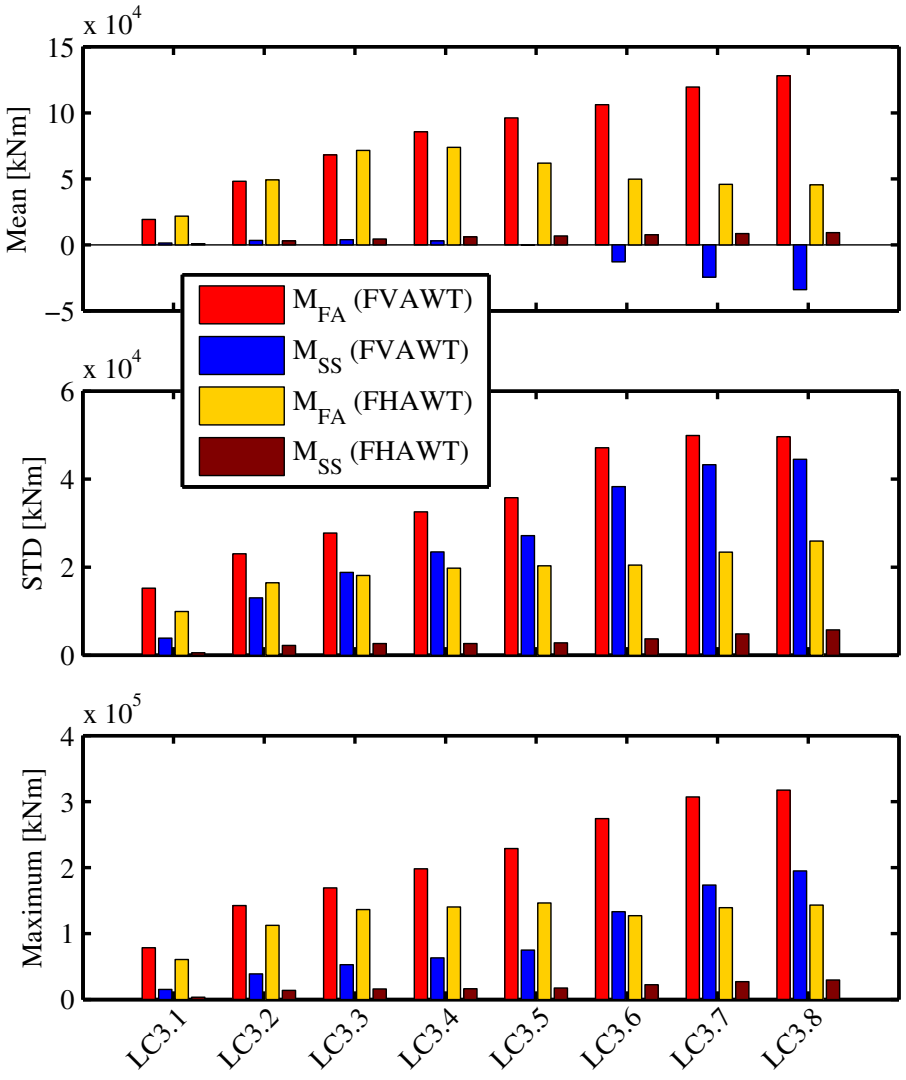

Figure 12: Mean values, standard deviation and maximum value of the tower base fore-aft bending moment (M_{FA}) and side-to-side bending moment (M_{SS}) for the FHAWT and FVAWT

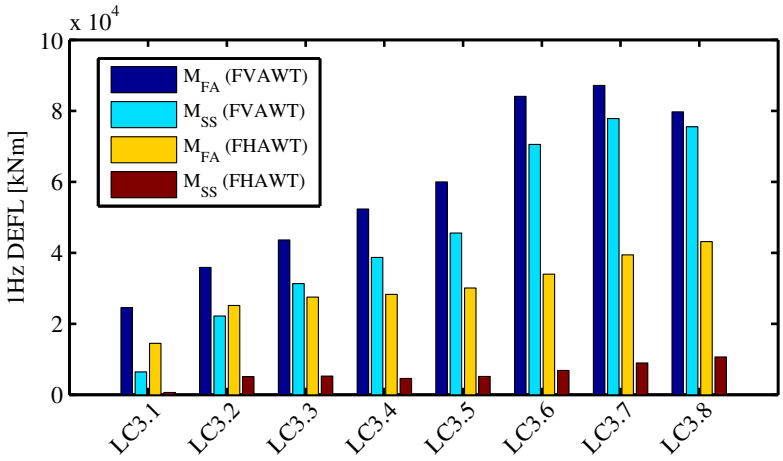

Figure 13: 1 Hz damage equivalent fatigue loads (DEFLs) of the tower base fore-aft bending moment (M_{FA}) and side-to-side bending moment (M_{SS}) for the FHAWT and FVAWT

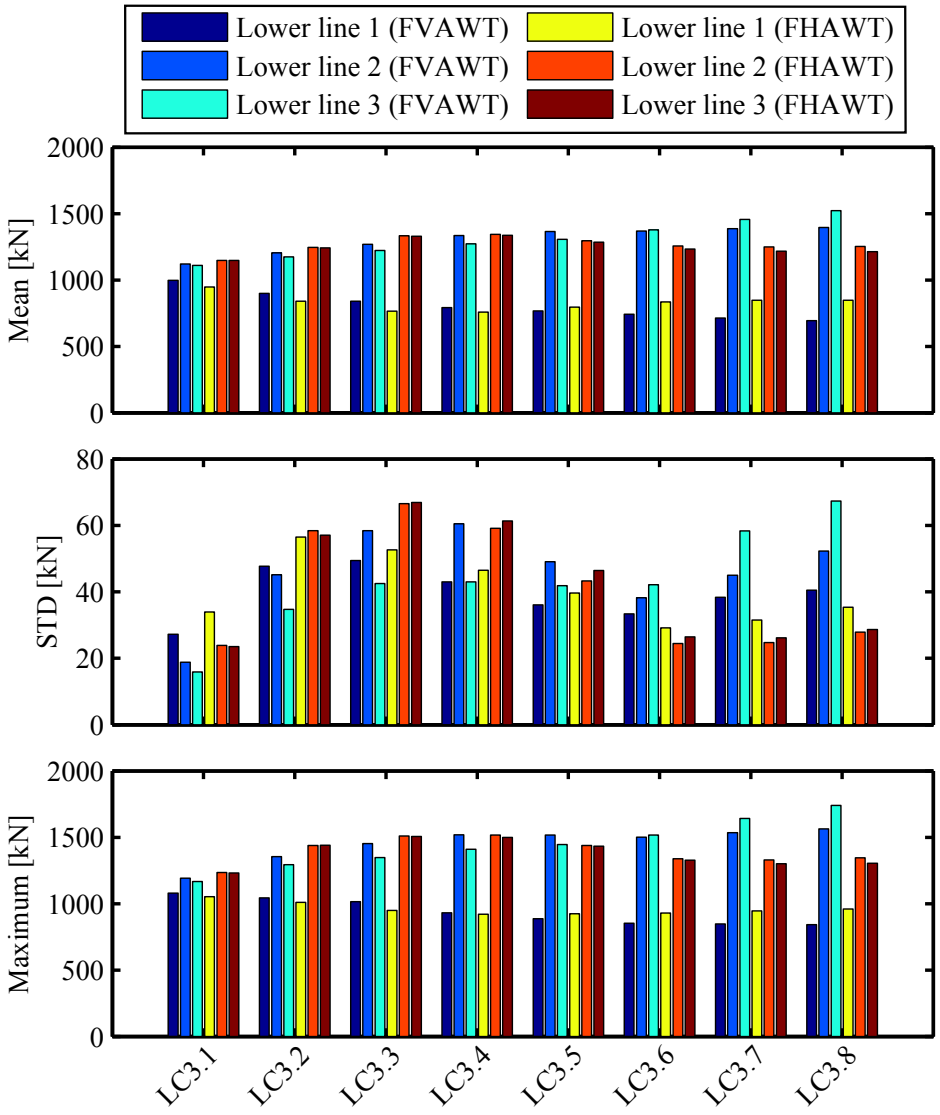

Figure 14: Mean values, standard deviation and maximum values of the tension in the lower lines for the FHAWT and FVAWT

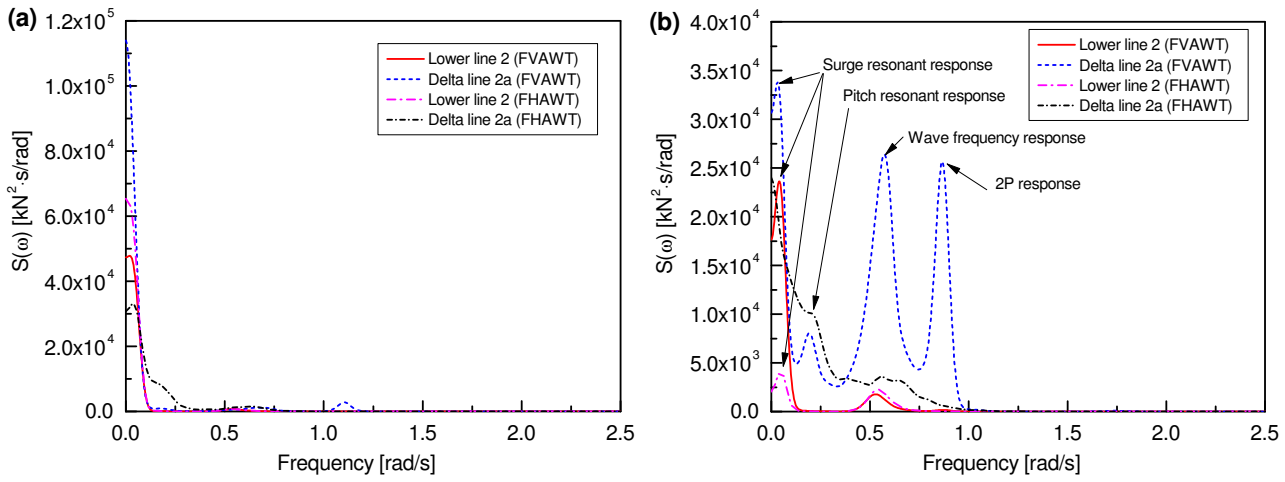

Figure 15: Power spectra of the tension in lower line 2 and delta line 2a for the FHAWT and FVAWT in (a) LC3.3 with $U_w = 10\ m/s$ and (b) LC3.7 with $U_w = 22\ m/s$.

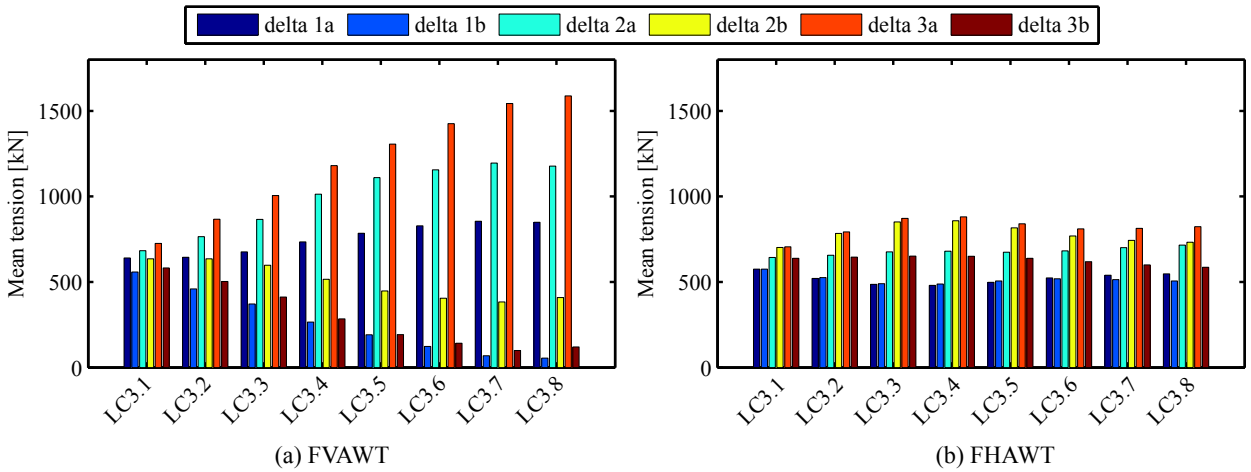

Figure 16: Mean values of the tension in the delta lines for the FHAWT and FVAWT

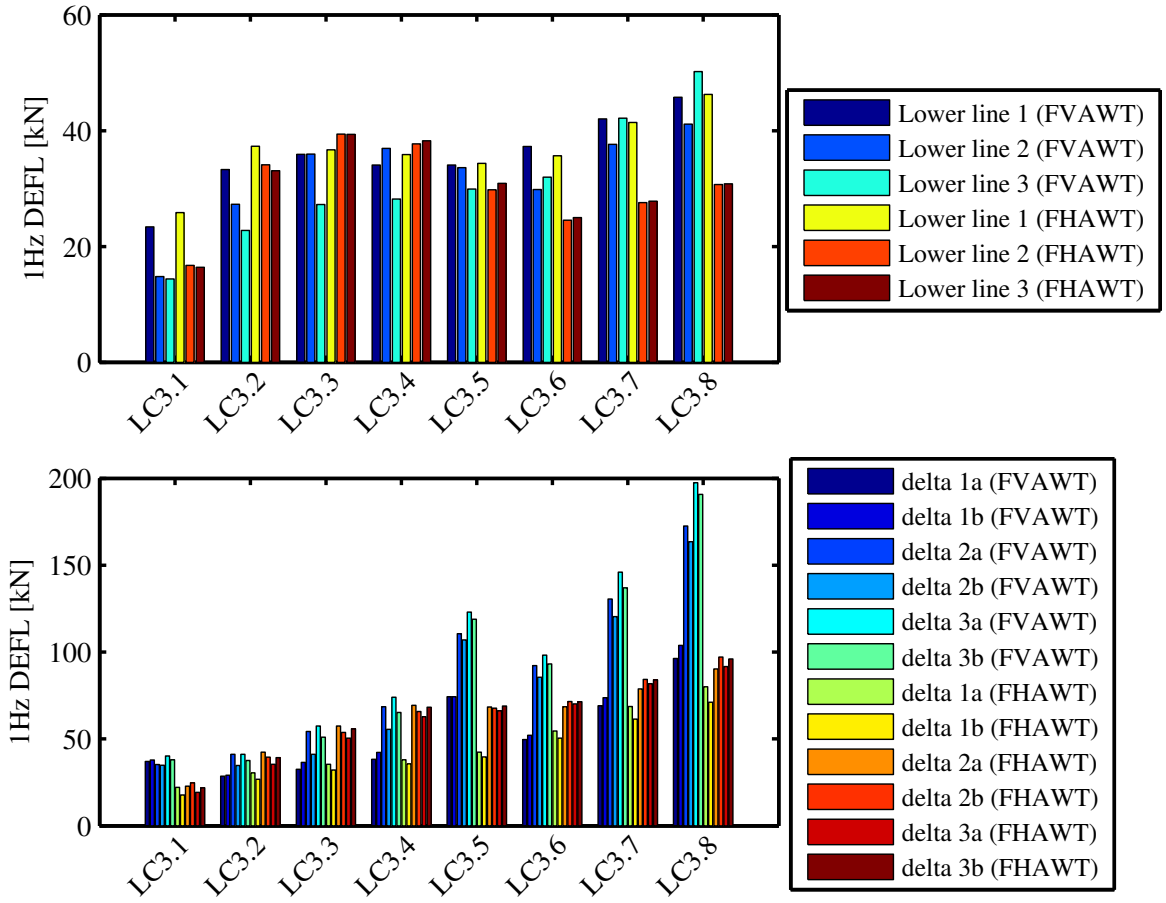

Figure 17: 1 Hz damage equivalent fatigue loads (DEFLs) of the tension in the lower lines and delta lines for the FHAWT and FVAWT

List of Tables

Table 1: Specifications of HAWT and VAWT

Turbines	FVAWT	FHAWT
Rated power [MW]	5	5
Rotor radius [m]	63.74	63
Rotor height/hub height [m]	129.56	90
Chord [m]	7.45	1.419-4.652
Cut-in, rated, cut-out wind speed [m/s]	5 , 14 , 25	5 , 11.4 , 25
Rated rotor rotational speed [rpm]	5.26	12.1
Nacelle mass [kg]	0	240,000
Rotor mass [kg]	305,044	110,000
Shaft mass/Tower mass [kg]	449,182	249,718
Location of overall CM [m]	(0 , 0 , 75.6)	(-0.2 , 0 , 70.06)

Table 2: Properties of the floating wind turbine systems

Floater	FVAWT	FHAWT
Water depth [m]	320	320
Draft [m]	120	120
Diameter at MWL [m]	6.5	6.5
Platform mass, including ballast [ton]	7308.29	7466.33
Center of mass for platform [m]	(0, 0, -89.76)	(0, 0, -89.92)
Buoyancy in undisplaced position [kN]	80710	80710
Center of buoyancy [m]	(0, 0, -62.07)	(0, 0, -62.07)
Surge/Sway natural period [s]	130.8	130.4
Heave natural period [s]	27.3	31.5
Pitch/Roll natural period [s]	34.5	29.6
Yaw natural period [s]	8.5	8.2

Table 3: Load Cases –steady wind only conditions

	U_w [m/s]	Wind Cond.	Sim. Length [s]
LC1.1	5	NWP	800
LC1.2	10	NWP	800
LC1.3	14	NWP	800
LC1.4	18	NWP	800
LC1.5	22	NWP	800
LC1.6	25	NWP	800

Table 4: Load Cases –turbulent wind only conditions

	U_w [m/s]	Wind Cond.	Sim. Length [s]
LC2.1	5	NWP+NTM	3600
LC2.2	10	NWP+NTM	3600
LC2.3	14	NWP+NTM	3600
LC2.4	18	NWP+NTM	3600
LC2.5	22	NWP+NTM	3600
LC2.6	25	NWP+NTM	3600

Table 5: Load Cases –combined wind and waves

	U_w (FVAWT) [m/s]	U_w (FHAWT) [m/s]	H_s [m]	T_p [s]	Wind Cond.	Sim. Length [s]
LC3.1	5	5.09	2.10	9.74	NWP+NTM	3600
LC3.2	8	8.14	2.55	9.86	NWP+NTM	3600
LC3.3	10	10.17	2.88	9.98	NWP+NTM	3600
LC3.4	12	12.20	3.24	10.12	NWP+NTM	3600
LC3.5	14	14.24	3.62	10.29	NWP+NTM	3600
LC3.6	18	18.31	4.44	10.66	NWP+NTM	3600
LC3.7	22	22.37	5.32	11.06	NWP+NTM	3600
LC3.8	25	25.43	6.02	11.38	NWP+NTM	3600